Chemical and Process Engineering: New Frontiers, 2026, 47(1), e126
DOI: 10.24425/cpe.2026.158124

Modelling drug release from a hydrogel carrier into the infected gingival mucosa

Tomasz Grygier, Maciej Grabowski, Edward Kijak, Anna Trusek

Wroclaw University of Science and Technology, Wybrzeze Wyspianskiego 27, 50-370 Wroclaw, Poland

* **Corresponding author, e-mail:** tomasz.grygier@pwr.edu.pl

Presented at
XIV Polish Conference
on Multiphase Flows
13–15 September 2025,
Gdańsk, Poland.
Guest Editor:
Donata Konopacka-Łyskawa

Article info:
Received: 15 September 2025
Revised: 20 November 2025
Accepted: 09 February 2026

Abstract
The paper presents a model of drug penetration into infected gingival mucosa via hydrogel overlays, which can be fully or partially covered with a polymer with limited permeability. The general geometry of the single drug carrier (single hydrogel overlay) was proposed as a flat cuboid with a triangular base. The number of overlays depends on the size of the infected area.
The model assumptions were formulated to account for the unsteady diffusion of the component within the carrier, the tissue, and the biofilm formed by pathogens, as well as for diffusion and convective transport in the liquid phase. The system of corresponding differential equations was solved using CFD methods.
Based on the modelling, the influence of key parameters such as polymer coverage of the carrier and hydrogel layer thickness was determined. It was demonstrated that external carrier coverage is crucial for effective, long-term therapy. Simulations showed that impermeable surfaces facing saliva slowed release by over 9-fold. Rendering those surfaces impermeable is especially desirable as the flow velocity increases. The distribution of the ingredient mass between system domains depends substantially on geometry, with hydrogel thickness influencing release dynamics.

Keywords
drug release, hydrogel carrier, mathematical modelling, CFD, periodontitis

1. INTRODUCTION

Periodontal disease affects the tissues that both surround and support the teeth. In advanced stages, the changes affect the bone and periodontal ligaments, ultimately leading to loosening and tooth loss (Lasserre et al., 2018; Patini et al., 2018). According to the WHO report from March 2025, it is estimated to have affected more than 1 billion cases worldwide (World Health Organization, 2025). The peak incidence of advanced periodontitis occurs around the age of 38. It corresponds to the maximum prevalence of the disease, which typically occurs around the age of 40 and remains at a steady level in subsequent years. In the group of Europeans aged 60-65, problems with periodontium affect 70-85% of people (Głowacka et al., 2019). The main risk factors for periodontal disease are poor oral hygiene and tobacco use (Głowacka et al., 2019; World Health Organization, 2025).

The current treatment phase involves deep cleaning of the affected area, as well as temporary or permanent tooth fixation (Abdullah et al., 2024). Since a thin layer of pathogens forming a biofilm remains on the surface, which cannot be reached mechanically, the therapy is supplemented pharmacologically (Budală et al., 2023). Antibiotics administered orally, intravenously, or intramuscularly disrupt the microflora throughout the body. Only a small portion of the drug reaches the actual site of inflammation. Therefore, whenever possible, local treatment is recommended for inflammatory conditions, including in dentistry. Local drug administration in the treatment of periodontal disease is complicated due to the terrain configuration and moist environment of the oral cavity. Furthermore, drug release from the carrier should occur over a relatively long period (several days/weeks), so the carrier must provide a sufficient reservoir of drug(s) for the duration of therapy. The challenge in delivering a drug to pathologically changed areas is to keep the drug at the target site while minimising the spread of the drug to other sites.

This paper describes an innovative drug carrier designed for the treatment of periodontal disease. It is based on a hydrogel structure that can be partially or fully coated with a polymer with limited drug permeability. The carrier's shape was adapted to the structure of the interdental spaces, which can be attributed to the form of a flat cuboid with a triangular base – Fig. 1. The carrier is printed using a 3D bioprinter at a size depending on the patient's and at a thickness selected for its mechanical and transport properties. The number of overlays depends on the size of the infected area.

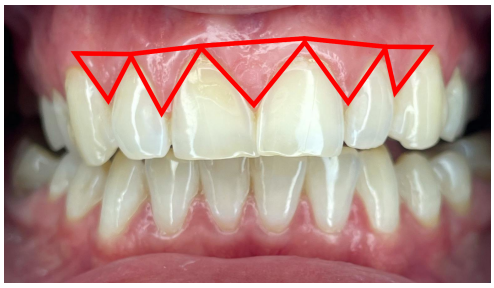

Figure 1. Geometric approximation of the anatomical shapes of the hydrogel carrier.

Accurately describing the transport phenomena accompanying release is crucial for selecting appropriate carrier parameters to achieve the most effective therapy (Siepmann and Siepmann, 2012). The method that enables such description, and therefore the proposal of practical solutions, is the construction of mathematical models. These models must accurately represent reality while remaining simple and general (Wang and Zhang, 2010).

The hydrogel overlay operates under conditions of constant saliva wetting, which adversely affects the effectiveness of drug delivery to the target site. It is crucial to adapt the carrier's geometry and prefabrication method to minimise drug losses. That allows for the possibility of coating the hydrogel layer with an additional polymer layer with limited drug permeability (Trusek et al., 2023). In the mathematical description of the system, this corresponds to limiting (and in extreme cases blocking) drug transport through a portion of the structure.

Based on the previous context, there is a need for a model that allows rapid estimation of release profiles for different shapes of the system. It is also important to be able to estimate the order of magnitude of the pathogen layer saturation times depending on the hydrogel overlay configuration.

2. THE MODEL FORMULATION

In general, drug transport within the carrier, pathogen layer (biofilm), and tissue is an example of unsteady mass diffusion. Mass transfer between individual zones of the system (Fig. 2, Fig. 3) is diffusive or convective (advection) in the case of flowing saliva. Furthermore, drug adsorption can occur within the biofilm layer. An elimination reaction of the drug in the biofilm and tissue is possible. For these conditions, the following assumptions are proposed:

1. A single hydrogel overlay with a volume of V_H has a cuboid geometry with a triangular base. The number of overlays is $n \geq 1$.
2. Drug transport within the hydrogel carrier can be described by the general equation of unsteady mass diffusion:

$$\frac{\partial c_i}{\partial t} = \frac{\varepsilon_H}{\tau_H} \cdot D_{i,H} \cdot \nabla^2 c_i \tag{1}$$

the concentration of the component is a function of time and position in the three-dimensional space of the system: $c_i = f(t, x, y, z)$;
3. Drug transport within the tissue is characterised by unsteady mass diffusion with possible I-order reaction eliminating it (conversion and/or vascular system uptake) from the system:

$$\frac{\partial c_i}{\partial t} = \frac{\varepsilon_T}{\tau_T} \cdot D_{i,T} \cdot \nabla^2 c_i - k_{i,RT} \cdot c_i \tag{2}$$

where $k_{i,RT}$ is kinetic constant.

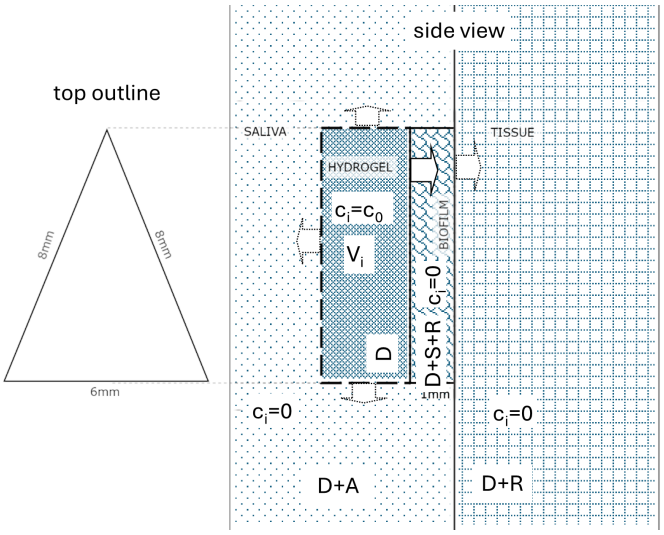

Figure 2. Schematic of the model system. D represents the diffusive region, D+R the diffusive-reactive region, D+S+R the diffusive-adsorptive-reactive region, and D+A the diffusive-convective region; initial drug concentrations and transport directions are indicated – desired transport shown by solid line arrows and undesired transport by dashed line arrows.

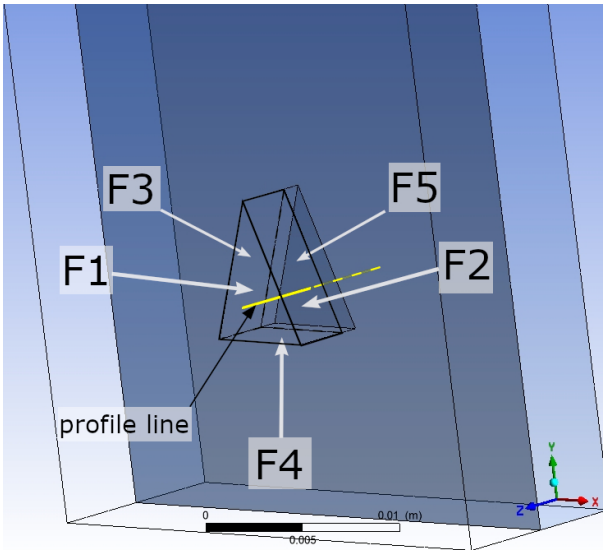

Figure 3. System geometry; marked line being the axis for concentration profiles depending on the z coordinate; marked surfaces/walls of the hydrogel overlay with numbering.

4. For saliva, which can move in laminar motion, the mass transport equation takes the form:

$$\frac{\partial c_i}{\partial t} = D_{i,S} \cdot \nabla^2 c_i - \dot{\nu} \cdot \nabla c_i \tag{3}$$

where $\dot{\nu}$ is the local fluid velocity vector, which is a function of time and position $\dot{\nu} = g(t, x, y, z)$.
5. The initial concentration of the component in the hydrogel overlay is equal to c_0.

6. The initial concentration of the component in the receiving phases (saliva, biofilm, tissue) is equal to 0.
7. The walls of the hydrogel overlay may have partial mass permeability or/and some of them may be impermeable.
8. The following processes can describe mass transfer from the depth of the overlay to the remaining phases:
   (a) diffusional mass transport within the hydrogel overlay with porosity, ε_H, and tortuosity, τ_H, to its walls, expressed by the diffusion coefficient, $D_{i,H}$,
   (b) diffusional and convective mass transport from the walls of the overlay to the depth of the liquid phase, which is saliva, remaining at rest or moving in laminar flow,
   (c) mass transfer from the hydrogel overlay to the adjacent biofilm by diffusion,
   (d) diffusional and convective mass transport from the biofilm walls to saliva in areas not in contact with the hydrogel overlay,
   (e) diffusional mass transport within the biofilm layer with porosity, ε_B, and tortuosity, τ_B, described by the diffusion coefficient, $D_{i,B}$,
   (f) diffusional and convective mass transport from saliva to the mucosa, which constitutes the first layer of tissue (the mucosa is attached to the tissue),
   (g) transfer of mass from the biofilm to the mucosa by diffusion
   (h) diffusional mass transport within the tissue, described by the diffusion coefficient, $D_{i,T}$, porosity, ε_T, and tortuosity, τ_T.
9. Adsorption of the component occurs in the biofilm layer as well as a reaction eliminating it (absorption to cells and/or conversion) from the system. This leads to the form of a transport equation containing terms related to adsorption, desorption and reaction:

$$\frac{\partial c_i}{\partial t} = \frac{\varepsilon_B}{\tau_B} \cdot D_{i,B} \cdot \nabla^2 c_i - k_{i,A} \cdot c_i \cdot \left(1 - \frac{q_i}{q_{i,\mathrm{MAX}}}\right) + k_{i,D} \cdot \frac{q_i}{q_{i,\mathrm{MAX}}} - k_{i,RB} \cdot c_i \quad (4)$$

where the constants $k_{i,A}$ and $k_{i,D}$ are the adsorption and desorption coefficients, respectively, q_i and $q_{i,\mathrm{MAX}}$ are the instantaneous and maximum concentration of the adsorbed component, respectively, related to the biofilm mass and $k_{i,RB}$ is I-order reaction kinetic constant.

The system is assumed to be isothermal and the diffusion coefficients to be independent of the component concentrations.

3. MATERIALS AND METHODS

Due to non-symmetricity of the modelled system and its multicomponent nature, CFD (computational fluid dynamics) numerical solution approach was employed. A geometry of a hydrogel overlay and its surroundings were prepared in DesignModeler and imported into ANSYS Fluent for meshing, both programs being part of a ANSYS software suite 2025R1. The flow and mass continuity, as well as momentum equations, were solved using finite-volume algorithms implemented in said software. The SIMPLE method was used with a pressure-based solver. A second-order upwind scheme was selected for pressure, momentum, and species-transport discretization.

The UDF (User Defined Functions) were prepared in C language to implement adsorbed mass values as UDS (User Defined Scalar) in biofilm region.

The parameters used in all simulations are presented in Table 1.

Table 1. Simulation parameters.

Symbol	Description	Value / Units
	Adsorption parameters	
q_{MAX}	Maximum adsorbed concentration in biofilm	$1.0 \cdot 10^{-1}$ [kg/m^3]
k_A	Adsorption coefficient	$1.0 \cdot 10^{-3}$ [1/s]
k_D	Desorption coefficient	$1.0 \cdot 10^{-6}$ [kg/m^{3}s]
	Transport parameters	
D_S	Saliva diffusion coefficient	$5.0 \cdot 10^{-10}$ [m^2/s]
$\frac{\varepsilon_H}{\tau_H} \cdot D_H$	Apparent hydrogel diffusion coefficient	$4.75 \cdot 10^{-10}$ [m^2/s]
$\frac{\varepsilon_T}{\tau_T} \cdot D_T$	Apparent tissue diffusion coefficient	$1.0 \cdot 10^{-10}$ [m^2/s]
$\frac{\varepsilon_B}{\tau_B} \cdot D_B$	Apparent biofilm diffusion coefficient	$5.0 \cdot 10^{-11}$ [m^2/s]
	Kinetic parameters	
k_{RB}	Reaction constant in biofilm	$2.0 \cdot 10^{-2}$ [1/s]
k_{RT}	Reaction constant in tissue	$1.0 \cdot 10^{-1}$ [1/s]
	General data	
c_0	Initial concentration in the hydrogel overlay	$1.0 \cdot 10^{-3}$ [kg/m^3]
V_B	Volume of biofilm layer	$2.22 \cdot 10^{-8}$ [m^3]
V_H	Volume of a single hydrogel overlay	$6.67 \cdot 10^{-8}$ [m^3]
V_S	Volume of saliva computational zone	$4.41 \cdot 10^{-6}$ [m^3]
V_T	Volume of tissue computational zone	$4.50 \cdot 10^{-6}$ [m^3]

Saliva flow velocity was estimated according to the study on saliva secretion (Boros et al., 1999) and assumed to be constant over time (Moscicka-Studzinska and Ciach, 2012). The magnitudes of these values were based on the literature cited above. The effects of variable saliva flow characteristics on release characteristics from a hydrogel overlay are to be analysed in future studies.

The diffusion coefficient value was kept at constant level in all simulated cases; its value was a rounded up approximation of literature reported figures (Pjanović et al., 2010; Reinscheid, 2006; Stewart, 1996; Vrany et al., 1997). As a broad reference some well-known biological active ingredients were considered, like lidocaine hydrochloride at 37 °C, $D_{aq} = 1.38 \cdot 10^{-8}$ m^2/s (Pjanović et al., 2010), ciproflaxin at 37 °C, $D_{aq} = 0.69 \cdot 10^{-9}$ m^2/s (Stewart, 1996) and ciproflaxin at 25 °C, $D_{aq} = 5.63 \cdot 10^{-10}$ (Reinscheid, 2006). Also the values for metronidazole at 25 °C, $D_{aq} = 1.09 \cdot 10^{-9}$; ampicillin at 25 °C, $D_{aq} = 4 \cdot 63 \cdot 10^{-10}$ (Reinscheid, 2006) and levofloxacin at 21 °C, $D_{aq} = 2.28 \cdot 10^{-10}$ were known (Vrany et al., 1997).

Adsorption parameters in biofilm were assumed to be constant throughout the course of simulation even though it is known that in reality those are dynamic systems of high complexity (D'Acunto et al., 2016). The above assumption is based on the reasoning that the time-scale of changes of such a complex system characteristics (i.e. volume and porosity changes, species differentiation, composition of extracellular fluid and many more) is several magnitudes of order greater that the diffusion time-scale (Klapper and Dockery, 2010; Picioreanu et al., 2000). Thus, they were not considered in the presented model. The exact values of the adsorption and desorption coefficients were estimated based on literature-reported findings (Vrany et al., 1997). It was assumed that simulated ingredient binds to adsorption sites in 1:1 molar ratio.

The boundary conditions for diffusive species transport were set for each region separately and can be summarized as follows:

- no initial ingredient presence in saliva, biofilm or tissue:

$$c_i(x,y,z)_{t=0} = 0 \quad (\text{for each } x,y,z \subset R_S, R_B, R_T) \quad (5)$$

- initial concentration of an ingredient at hydrogel overlay set as per case:

$$c_i(x,y,z)_{t=0} = c_0 \quad (\text{for each } x,y,z \subset R_H) \quad (6)$$

where R_S, R_B, R_T and R_H are saliva, biofilm, tissue and hydrogel subsets of three-dimensional Cartesian space $\boldsymbol{R}^3$, respectively.

4. RESULTS

The model solutions were presented as concentration contours on selected planes running through the simulated 3D geometry of the system (Fig. 3). To show the obtained concentration profiles as a function of the z coordinate, a line (marked in yellow – Fig. 3) was selected running around the geometric centre of all zones. To estimate the efficiency of transport into the biofilm, the component masses in each zone were counted in subsequent simulation steps.

A closed system, in which the mass of the component that left the carrier accumulates in the receiving phases, and an open system, in which saliva flows in and out of the system, corresponding to the conditions in the oral cavity, was considered. In both cases, the effect of complete restriction of mass transport on selected surfaces of the hydrogel overlay on the obtained simulation results was examined.

Model solutions illustrating the dependence of mass transport on the relative sizes of the hydrogel and biofilm layers were also presented.

In all cases, it was assumed that there was only one ($i = 1$) diffusing component.

A summary of the results is presented in visualizations of concentration contours (Fig. 4) and concentration profile graphs (Fig. 5). The individual cases are discussed below. Key figures are also summarised in Table 2.

4.1. Case of an overlay with identical permeability through all walls

4.1.1. Salivary flow rate $v = 0.0$ [mm/s]

First, a simulation of the release of the substance from the overlay was performed without limiting the permeability of the mass. Therefore, none of the walls of the presented overlay geometry (Fig. 3) constituted a barrier to the diffusing compound. The solutions for this case, in the form of contours in the XY plane, running through the interface between the hydrogel and the biofilm, are presented in the visualisation (Fig. 4a).

The concentration of the component quickly equalises throughout the plane and, after 30 minutes have passed, begins to lose its characteristic, original contour resulting from the overlay shape. It is confirmed by the obtained concentration profiles along the z-axis of the system (line marked in Fig. 3), running through its conventional centre. A characteristic asymmetry in the concentration profiles on both sides of the hydrogel can be observed (Fig. 5a).

Table 2. Release characteristics from hydrogel overlay at an initial concentration of ingredient $c_0 = 1.0$ g/L.

Saliva phase	Stationary		Flowing $v = 0.1$ mm/s	
Overlay walls	no walls blocked	partially blocked	no walls blocked	partially blocked
Release time t_{90} [h]	3.6	20.5	0.35	3.2
Peak biofilm concentration [g/L]	0.30	0.36	0.12	0.17

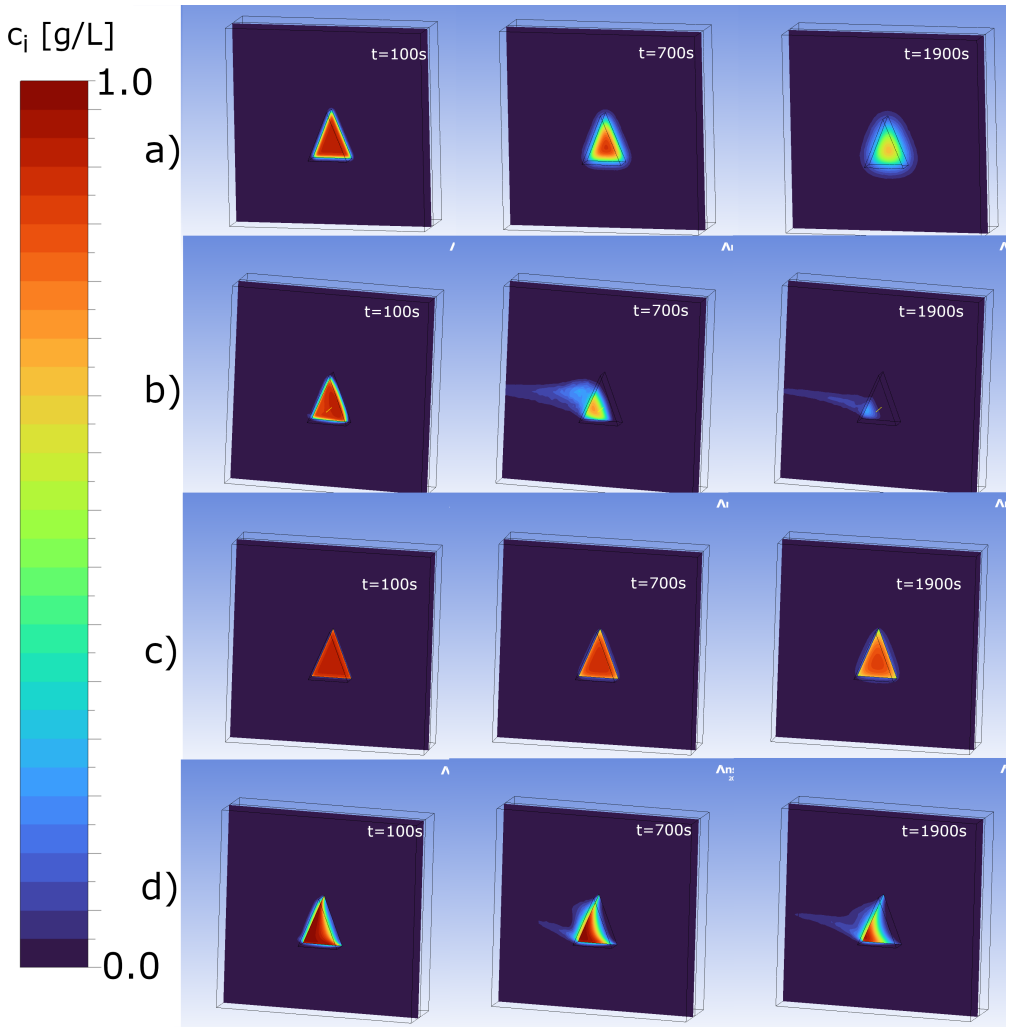

Figure 4. Contours of drug concentrations on the XY plane passing through the surface of contact of the overlay with the biofilm; a) stationary saliva layer without blocking mass transfer to saliva; b) saliva flow $v = 0.1$ mm/s without blocking the walls; c) stationary saliva layer, walls F1, F2, F3, F4 blocked; d) saliva flow $v = 0.1$ mm/s, walls F1, F2, F3, F4 blocked.

This is primarily due to the release of the ingredient into saliva through the side walls of the overlay (F2, F3, F4). The profile on the fluid side flattens much more quickly than on the biofilm side, where mass transfer occurs exclusively through a single, shared contact surface. The graph shows the concentrations on the left side (saliva) become higher significantly faster than on the right side (biofilm), indicating that the substance escapes from the hydrogel primarily into the surrounding fluid.

The following graph shows a sharp rise in the average concentration of the component in saliva (Fig. 6). Due to the high total volume of this component, this also indicates a high overall mass accumulated in it. It can also be observed that after the initial increase in the amount of the substance in the biofilm, the concentration decreases. It is primarily the result of further diffusion of the modelled compound into the tissue and saliva. In the absence of convective flow and wall blocking, the effect of saliva saturation with the component is noticeable after approximately 2.7 hours.

After approximately 3.6 hours, the average ingredient concentration in the hydrogel drops more than 90% compared to its initial value of 1 g/L. After 10 minutes, the average concentration of the substance in the biofilm reaches a maximum of 0.30 g/L, then drops steadily. Free diffusion of the mass into saliva significantly reduces the ingredient's residence time and availability in the biofilm.

4.1.2. Saliva flow velocity $v = 0.1$ [mm/s]

In the simulation conducted with flow (Fig. 4b), a characteristic blurring of the contours is observed. This time, however, as the mass of the flowing fluid moves across the overlay, the molecules of the modelled compound are dispersed over a much larger area in the direction of the fluid's velocity vector.

Compared to saliva at rest (Fig. 5a), the concentration profile is much steeper (Fig. 5b). Average concentrations in a given space across all zones reach low values much faster. Significant mass washout from the system is noticeable (shorter abscissa – Fig. 7).

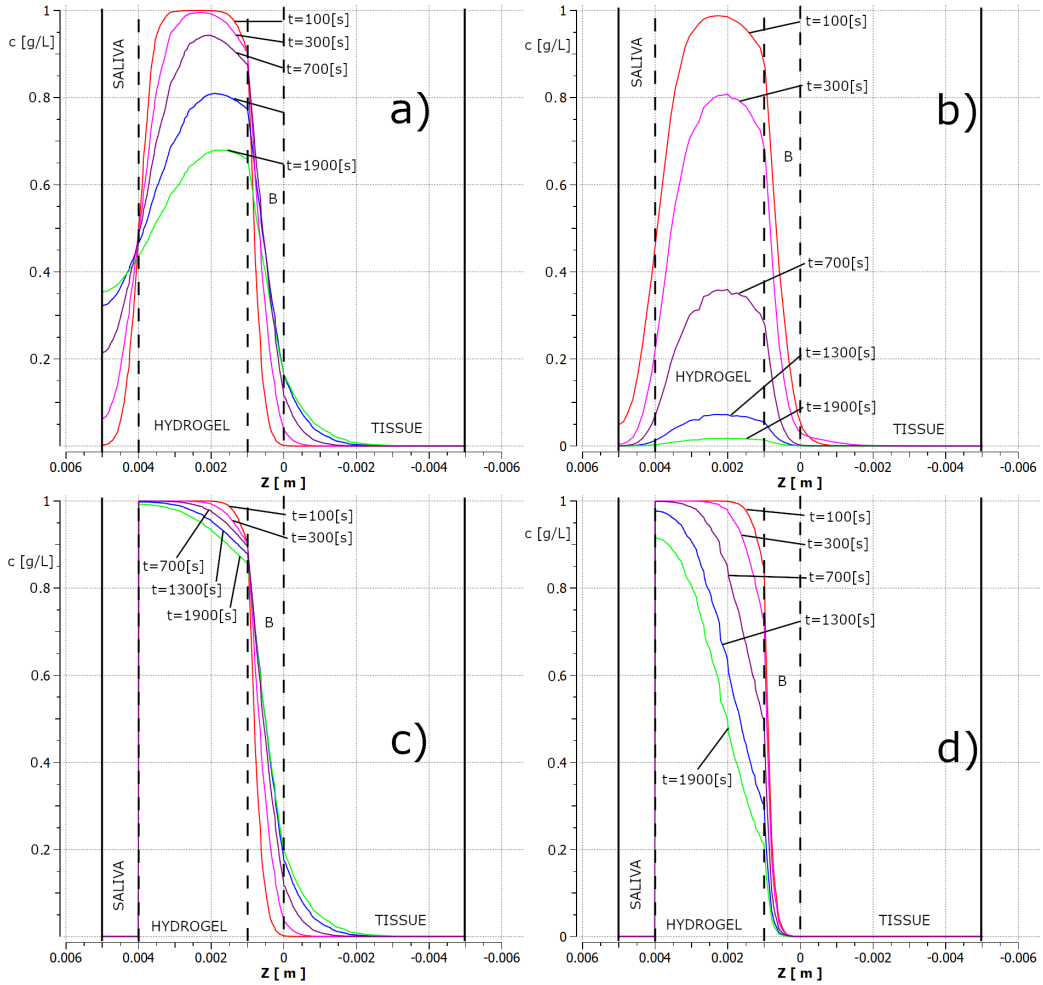

Figure 5. Concentration profiles on the selected line in the z-axis for different simulation durations (the z-axis is inverted to achieve consistency with the presented 3D visualisations). a) stationary saliva – no wall blocking; b) saliva flow $v = 0.1$ mm/s – no wall blocking; c) stationary saliva – walls F1, F2, F3, F4 blocked; d) saliva flow $v = 0.1$ mm/s – walls F1, F2, F3, F4 blocked.

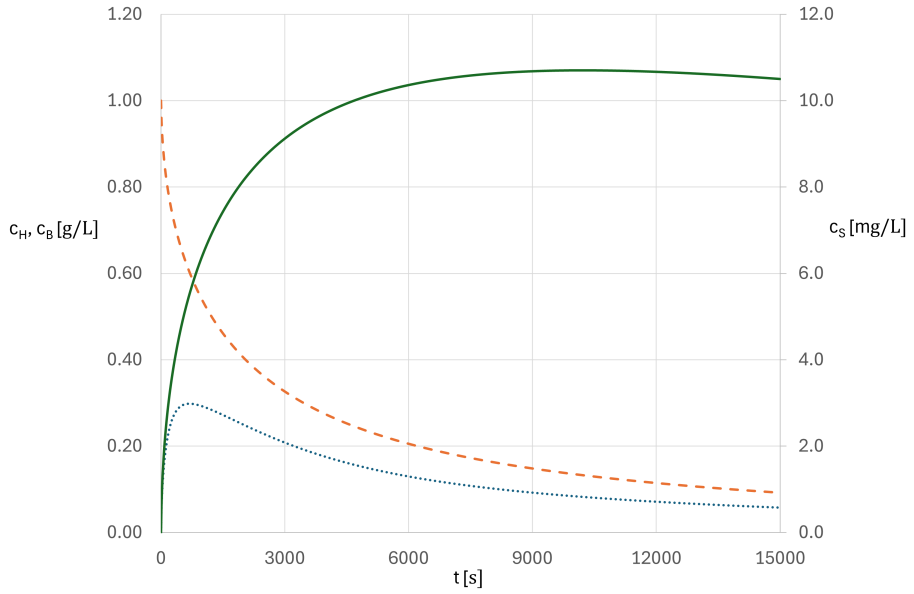

Figure 6. Changes in the average concentration of the component found in saliva (continuous line – auxiliary axis), overlay (dashed line) and biofilm (dotted line) as a function of time; saliva flow $v = 0.0$ mm/s – no blocking of the walls.

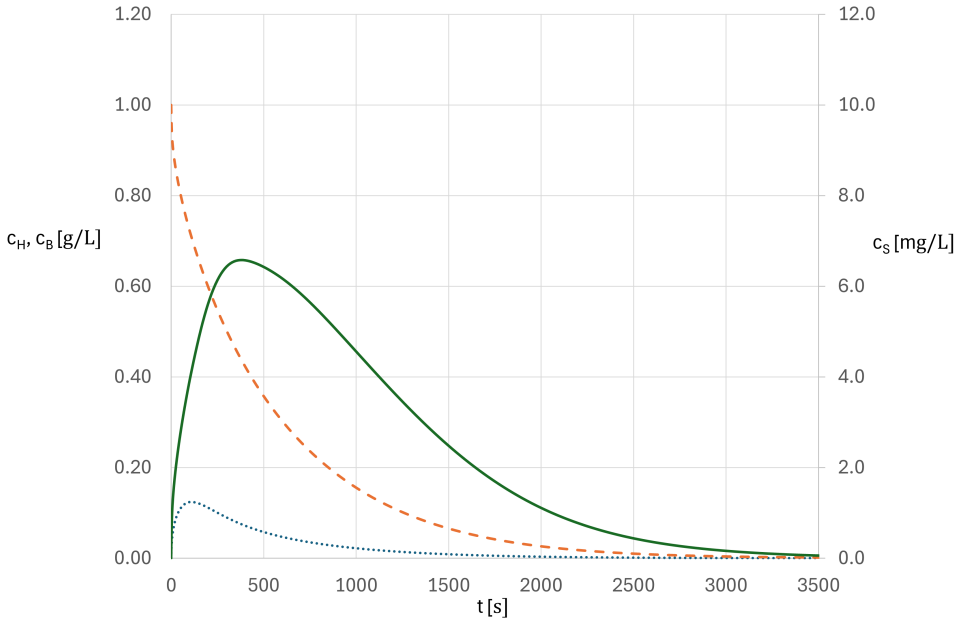

Figure 7. Changes in the average concentration of the component found in saliva (continuous line – auxiliary axis), overlay (dashed line) and biofilm (dotted line) as a function of time; saliva flow $v = 0.1$ mm/s – no blocking of the walls.

The component's concentration in saliva reaches a maximum, then decreases noticeably. It is mainly associated with the substance leaving the system with the moving fluid (Fig. 7). In both cases (Fig. 6 and Fig. 7), average concentration changes in the biofilm and hydrogel are similar in nature, yet in the case of forced flow they occur faster.

In less than 21 minutes, 90% of the ingredient is already released outside the overlay. It is over 10 times faster than previously. The peak average concentration in the biofilm occurs after only 1.5 minutes, at 0.12 g/L. Afterwards, this time value diminishes rapidly. The flowing liquid can significantly reduce the biofilm's saturation with the delivered substance.

4.2. The case of an overlay with modified permeability through selected walls

4.2.1. Salivary flow rate $v = 0.0$ [mm/s]

Blocking all surfaces (F1, F2, F3, F4 – Fig. 3), except for the one in direct contact with the biofilm (F5 – Fig. 3), for example, by covering them with an impermeable polymer, significantly slows the release of substances into the saliva (Fig. 4c).

When the fluid surrounding the overlay is stationary, the resulting contours are similar to those obtained for the first case discussed (Fig. 4a). However, the substance content at individual points in the system differs significantly. In the time-varying local concentration profiles, a prevailing transport towards the biofilm is evident (Fig. 5c). In the overlay, the shapes of the curves at similar time intervals indicate an increasing, directional slope. After blocking transport through selected walls, the averaged concentrations in the system's individual zones follow a slightly different pattern (Fig. 8).

The release of the substance from the overlay is slower than in the previously discussed cases. The average concentration profile in the biofilm demonstrates that the modelled compound persists longer.

Covering the walls of the overlay exposed to saliva (F1, F2, F3, F4) significantly reduces the overall release tempo. After 20.5 hours, 90% of the drug from the hydrogel is released. It is over 5 times longer than in a similar flow case without wall blocking. The content of the substance in biofilm reaches a peak value of 0.36 g/L after 21.7 minutes. It is slightly more and somewhat later than in the comparable case with fully permeable overlay sides. But after reaching the 90% release level in the previous case, the average drug concentration in the biofilm was only 0.066 g/L. After the same time, i.e. 3.6 hours, it is now 0.26 g/L. The biofilm saturation has significantly improved.

4.2.2. Saliva flow velocity $v = 0.1$ [mm/s]

In the following case, the solutions (Fig. 4d) were obtained for saliva moving at a constant linear velocity. The convective flow parameters were identical to those in the second case discussed (Fig. 4b). Simulations were performed with blocked mass transport as above (walls F1, F2, F3, and F4 blocked; wall F5, in contact with the biofilm, unblocked).

It was observed (Fig. 4d) that after 30 minutes, despite noticeable streaks of mass flowing away with the fluid, the concentration of the component at the interface between the

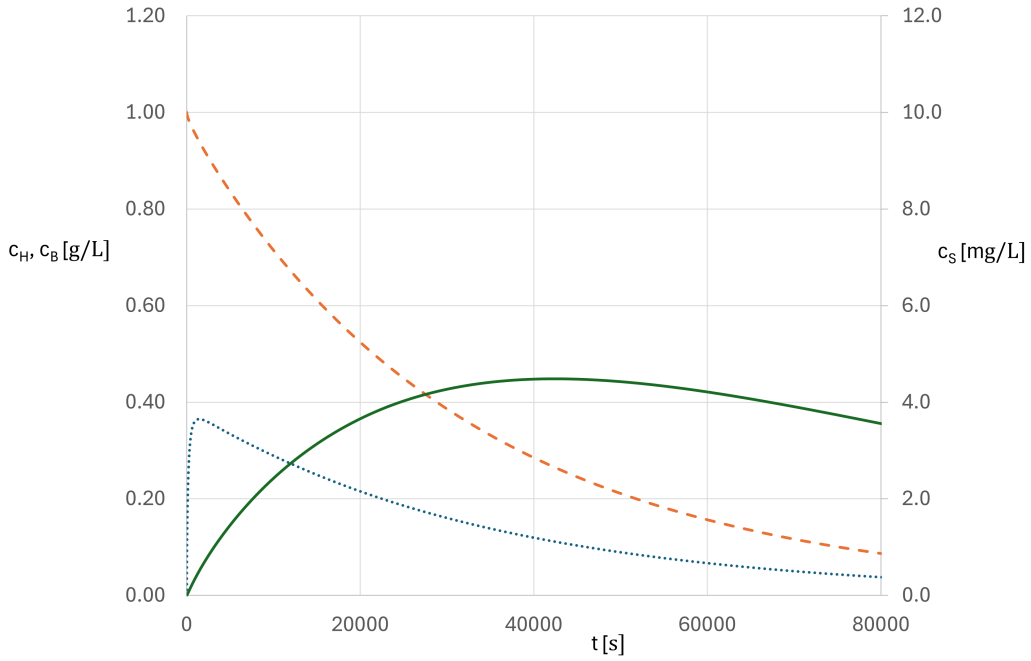

Figure 8. Changes in average concentrations of the component present in saliva (continuous line – auxiliary axis), overlay (dashed line) and biofilm (dotted line) as a function of time; saliva flow $v = 0.0$ mm/s – walls F1, F2, F3, F4 blocked;

hydrogel and the biomass was still significant. Preventing mass flow directly into the body fluid flowing over the overlay improves the availability of the substance feeding the biofilm layer (Fig. 5d). The time needed to achieve 90% release is 3.2 hours. It is almost 9 times longer than in a similar case, but without the overlay sides blocked for mass permeability. The peak mean concentration in the biofilm is 0.17 g/L, reached after 2.8 minutes. In a corresponding flow case without walls blocked after 50 minutes there is virtually no drug in the biofilm (Fig. 7). After the same time but with walls blocked the average concentration in the biofilm is 0.073 g/L (Fig 9).

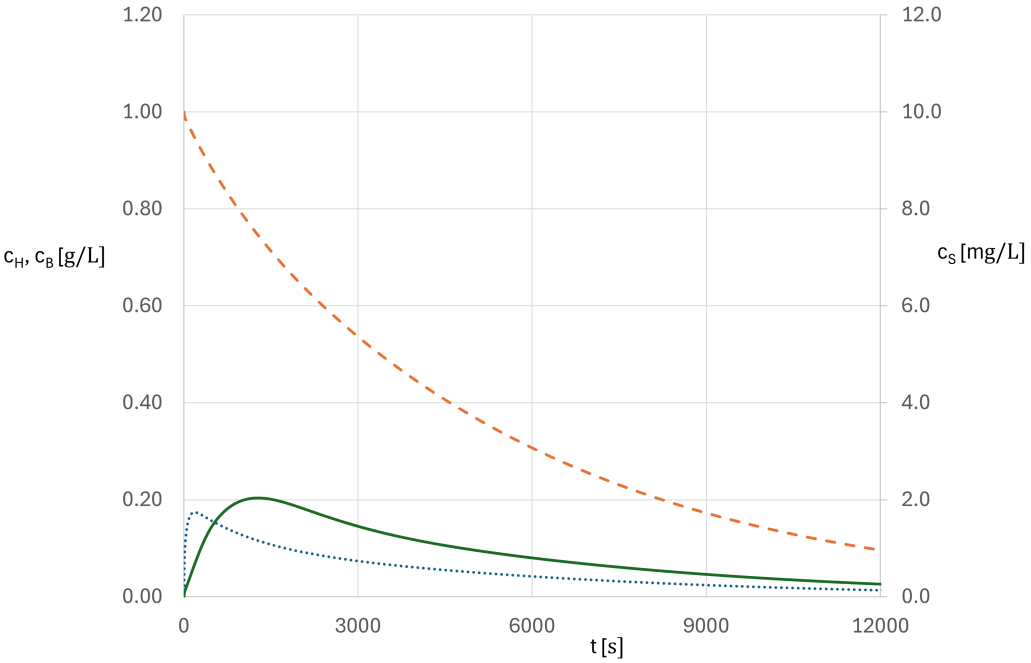

Figure 9. Changes in average concentrations of the component contained in saliva (continuous line – auxiliary axis), overlay (dashed line) and biofilm (dotted line) as a function of time; saliva flow $v = 0.1$ mm/s – walls F1, F2, F3, F4 blocked.

This is only half reduction of the peak concentration. At the same time a noticeable outflow of the substance from the system is observed, as evidenced by the characteristic maximum in the line describing the mean concentration of drug in saliva (Fig. 9).

4.3. The case of a varying overlay thickness

As the overlay thickness changes while maintaining the same concentration, the total amount of the component delivered to the system changes. It is important to compare the proportion of the initial component remaining in the biofilm over time. To answer this question, simulations were conducted for three different overlay thicknesses: 3 mm (the initial case – discussed above), 2 mm, and 1 mm. The remaining system parameters remained unchanged. In particular, the biofilm layer thickness maintained constant at 1 mm. Based on the previous observations, it was assumed that in further considerations it would be worthwhile to discuss the overlay configuration with blocked walls F1, F2, F3, and F4 and with unblocked wall F5, adjacent to the biofilm.

4.3.1. Overlay thickness 3 [mm]

As can be seen in the graph (Fig. 10a – dashed line), the average content in the hydrogel overlay gradually decreases over time. Comparing the cases with no walls blocked (Fig. 10d – dashed line) a significant increase in the component content can be observed. This observation is consistent with those made earlier. The biofilm layer also shows a tendency for more mass to be present at each release stage when walls are blocked (Fig. 10a vs 10d – solid lines). The characteristic shape of the curve, with a rapidly reaching maximum, is also noticeable.

4.3.2. Overlay thickness 2 [mm]

After reducing the thickness, a faster mass loss from the overlay is observed (Fig. 10b – dashed line). Comparing to one of the previously described cases, i.e., a 3 mm thick overlay and no walls blocked (Fig. 10d – dashed line), this is not as profound increase in release dynamics. The mean concentration curve in the biofilm is somewhat steeper after reaching the maximum (Fig. 10b – solid line). A general trend of early accumulation and gradual decline is conserved.

4.3.3. Overlay thickness 1 [mm]

The above observations are confirmed in the following discussed case with an even thinner thickness (Fig. 10c). The average concentration in the overlay is significantly lower than in previously discussed cases. Increase in mean concentration of the component is again noticeable in the biofilm at an early stage (Fig. 10c – solid line). Furthermore, a following decrease in the ingredient content in this zone is more significant.

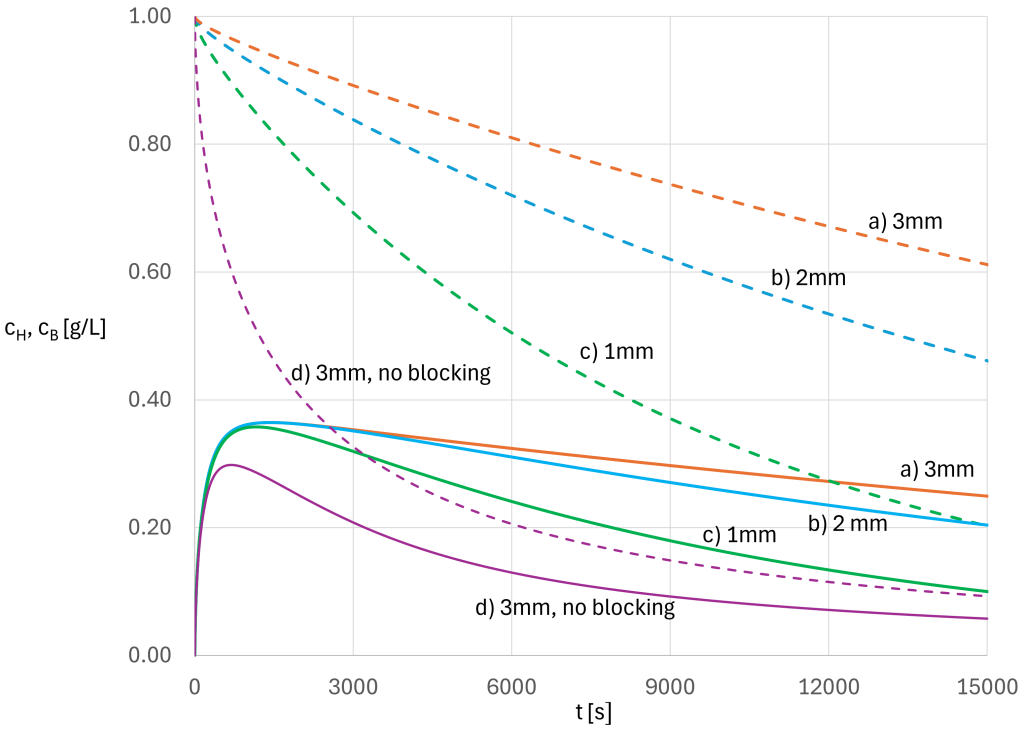

Figure 10. Changes in the average concentration of the component in the overlay (dashed line) and the biofilm (solid line) as a function of time for different conditions and system geometry; stationary saliva; cases discussed in the text.

The above results suggest that as the overlay thickness decreases, the fraction of mass entering and remaining in the biofilm, after reaching peak concentration, decreases more rapidly. The initial increase and peak concentrations of a component in the biomass are only slightly correlated with the relative volumes of the hydrogel and biofilm phases. It is clearly visible when compared with the biofilm concentration curve for the case with no walls blocking (Fig. 10d – solid line).

5. DISCUSSION

As the obtained solutions of the developed model demonstrate, the release of substances such as antibiotics from hydrogel carriers (overlays) is strongly dependent on the geometry of the system, rheological conditions, and above all, the permeability of the individual mass exchange surfaces. The effectiveness of any therapy depends on the ability to deliver drugs precisely to the affected areas. Ensuring drug saturation of the infected spaces for a sufficiently long time is also crucial. The desired state of the presented system is therefore one in which the saturation of the biofilm layer with the substance, relative to the other phases, is as high as possible.

The dynamics of substance release from the discussed structure varied significantly across different cases (Table 2). Notably, saliva flow had the most significant influence. At an assumed linear flow velocity of 0.1 mm/s, it decreased the release time as measured by t_{90} by a factor of 10.2, when no walls were blocked, and by a factor of 6.4, when there was a permeability modification. It also shows the importance of blocking treatment as a countermeasure against the outflow of the drug.

One of the goals of the presented work was to determine the influence of the specific triangular shape of the overlay's base. The visualisation of the transverse concentration contours (Fig. 11) below provides some insight into this subject.

As can be seen, the concentration contours resulting from the gradient across the biomass layer are very similar. Greater differences are visible in the concentration contours in the hydrogel, where the component depletes more rapidly – this is particularly pronounced in the thinner overlay (Fig. 11c). Finally, the difference in mass that has not yet flowed out of the overlay is very pronounced. The area marked in darkest red – corresponding to high concentrations – is largest in the thicker geometry (Fig. 10a). The observed contour outline, with lower concentrations at the top of the overlay, is a result of its relatively minor volume as the triangular shape of the base narrows.

In the model, the effects of possible mass adsorption in the biofilm layer are incorporated. An analysis of the adsorption parameter on release dynamics is shown in Figure 12.

The parameters were chosen to facilitate comparison of more significant adsorption ($q_{MAX} = 1.0\cdot$ [kg/m^3] and $k_D = 1.0 \cdot 10^{-7}$ [kg/m^{3}s] – Fig. 12b) and less critical ($q_{MAX} = 1.0 \cdot 10^{-2}$ [kg/m^3] and $k_D = 1.0 \cdot 10^{-5}$ [kg/m^{3}s] – Fig. 12b) than parameters chosen for main simulations, but still within reported figures (Chaumet et al., 2019; Wang et al., 2002). The differences in release and saturation become noticeable only after over 13 hours.

It is also expected that varying magnitudes of elimination kinetics will influence release and saturation profiles on a scale similar to that of adsorption characteristics. The actual effect remains to be confirmed in future work.

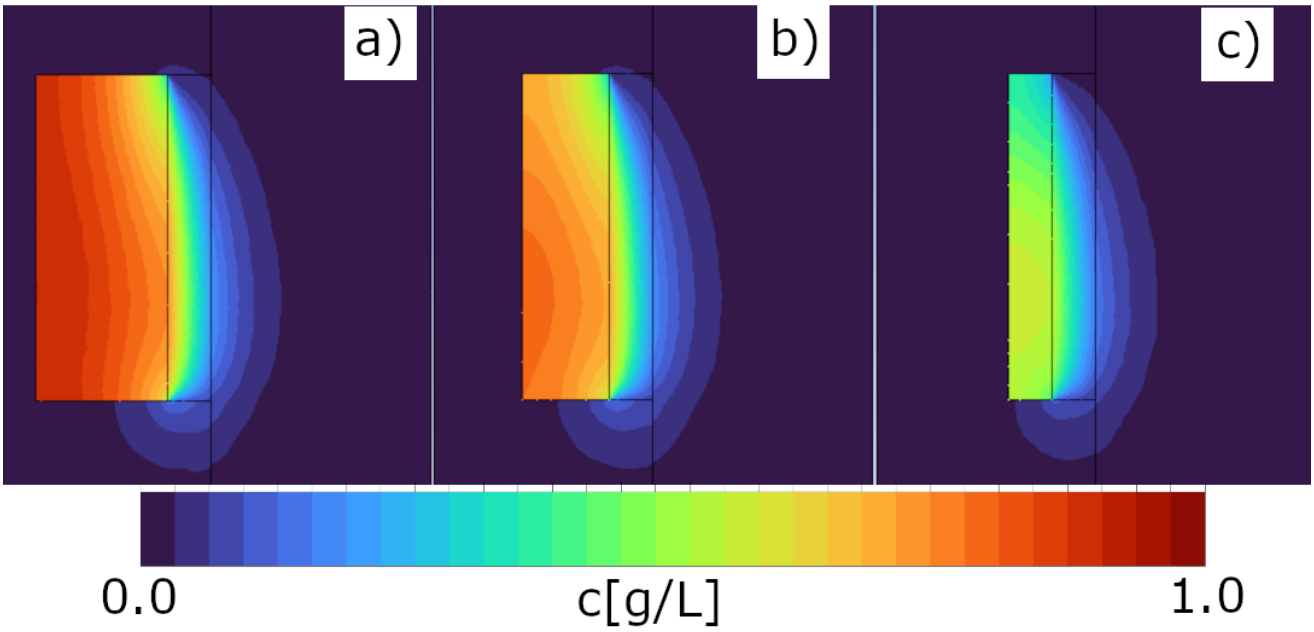

Figure 11. Contours of the concentrations in the YZ plane running through the centre of the overlay geometry after 100 minutes of simulation – walls on the saliva side blocked for mass transport; overlay thicknesses: a) 3 mm; b) 2 mm; c) 1 mm.

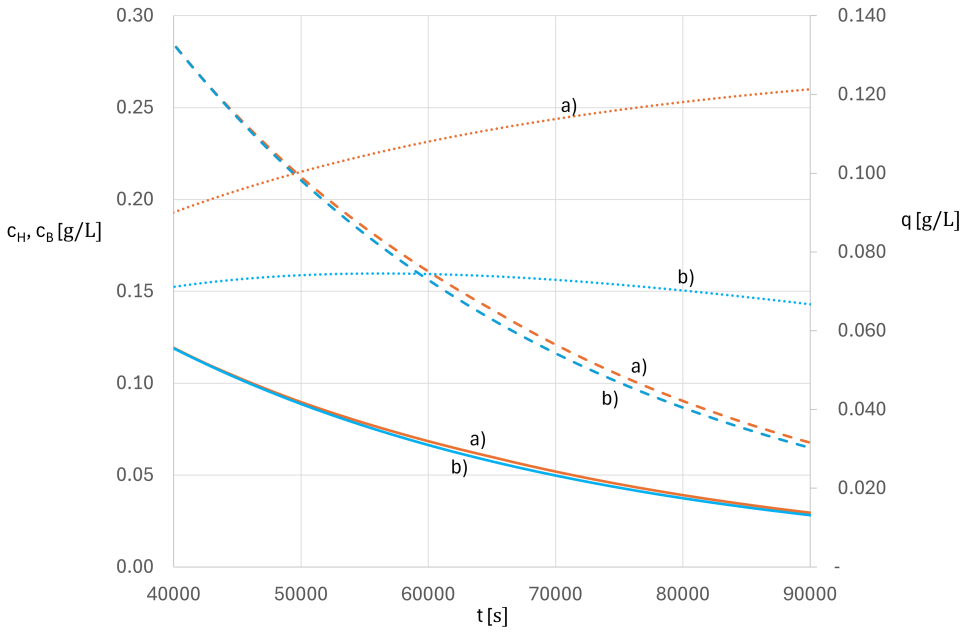

Figure 12. Changes in the average concentration of the component in the hydrogel overlay (dashed line), the biofilm (solid line) and mean adsorbed concentration (dotted line – auxiliary axis) as a function of time for different adsorption characteristic; stationary saliva; cases discussed in the text.

The simulation results are expected to change with the specific properties of the drug and to vary mainly with the magnitude and modification of the diffusion parameters and the walls' permeability. Yet the effectiveness of the polymer coating procedure on the hydrogel may not be 100%. It means that even on coated walls, some mass transfer will occur. It can be assumed that the resulting release effects will fall between the four cases mentioned above. It is also to be confirmed.

6. CONCLUSIONS

The proposed model enabled estimation of the relative release times of the substance from the carrier. It was observed that the profiles and contours of concentrations, on selected cross-sections of the flat cuboid with a triangular base-shaped hydrogel overlay, differed significantly depending on the degree of permeability restriction of its walls. Simulations showed that rendering the carrier's surfaces impermeable to saliva could result in an over 9-fold slowdown in release for selected diffusion, adsorption and reaction parameters. High salivary flow rates accelerate drug release from the hydrogel, thereby decreasing biofilm exposure to the drug. This effect is greater in the case of the hydrogel overlay walls with free mass permeability to saliva.

The distribution of the ingredient mass supplied by the carrier among the individual domains of the system is slightly less dependent on geometry. Smaller hydrogel overlay thickness does not significantly affect drug delivery to the biofilm at the initial stage. But it shortens the time of biofilm saturation.

Calculated concentration contours show that in the tapered areas of the hydrogel overlay, the supplied component is depleted faster. This means an uneven saturation of the target layer. Even in the most promising case shown, the total time to release is measured only in hours, not days. Making the hydrogel overlay an attractive therapeutic alternative would additionally require slowing down the release process. E.g., the hydrogel overlay could alter mass transfer characteristics at the surface where it contacts the biofilm. It will, however, be the next step in the research, i.e. limiting mass permeation of the hydrogel overlay into biofilm (an additional mass transfer resistance).

ACKNOWLEDGEMENTS

The research was funded by a grant NCN/PRELUDIUM BIS 2022/47/O/ST8/02850

SYMBOLS

V_H	volume of a single hydrogel overlay, m^3
t	time, s
n	number of overlays
c_i	concentration of the component i, mg/L, g/L, kg/m^3
c_0	initial concentration of the component in the hydrogel overlay, g/L, kg/m^3
q_i	instantaneous concentration of the adsorbed component in the biofilm, g/L, kg/m^3
$q_{i,MAX}$	maximum concentration of the adsorbed component in the biofilm, g/L, kg/m^3

D_{aq}	diffusion coefficient of reference substances is water, m^2/s
$D_{i,j}$	diffusion coefficient of the component in a given phase, m^2/s
ε_H	porosity of the hydrogel, –
ε_B	porosity of the biofilm, –
ε_T	porosity of the tissue, –
τ_H	tortuosity of the hydrogel, –
τ_B	tortuosity of the biofilm, –
τ_T	tortuosity of the tissue, –
$k_{i,A}$	adsorption coefficient in the biofilm, *1/s*
$k_{i,D}$	desorption coefficient in the biofilm, kg/m^3s
$k_{i,RB}$	reaction kinetic constant in the biofilm, 1/s
$k_{i,RT}$	reaction kinetic constant in the tissue, 1/s
$\dot{\nu}$	local velocity vector of saliva, m/s

Geometry indicators

R_H	domain of the hydrogel
R_B	domain of the biofilm
R_T	domain of the tissue
R_S	domain of saliva
F1, F2, F3, F4	overlay walls in contact with saliva
F5	overlay wall in contact with the biofilm

Subscripts

1	number of component
aq	aqueous
j	denotes domain, either (B)iofilm, (T)issue, (H)ydrogel or (S)aliva
90	denotes time at which 90% of the drug has been released from the carrier

REFERENCES

Abdullah F.M., Hatim Q.Y., Oraibi A.I., Alsafar T.H., Alsandook T.A., Lutfi W., Al-Hussaniy H.A., 2024. Antimicrobial management of dental infections: updated review. *Medicine*, 103, e38630. DOI: 10.1097/MD.0000000000038630.

Boros I., Keszler P., Zelles T., 1999. Study of saliva secretion and the salivary fluoride concentration of the human minor labial glands by a new method. *Arch. Oral Biol.*, 44, S59–S62. DOI: 10.1016/s0003-9969(99)90022-5.

Budală D.G., Luchian I., Tatarciuc M., Butnaru O., Armencia A.O., Virvescu D.I., Scutariu M.M., Rusu D., 2023. Are local drug delivery systems a challenge in clinical periodontology? *J. Clin. Med.*, 12, 4137. DOI: 10.3390/jcm12124137.

Chaumet B., Morin S., Boutry S., Mazzella N., 2019. Diuron sorption isotherms in freshwater biofilms. *Sci. Total Environ.*, 651, 1219–1225. DOI: 10.1016/j.scitotenv.2018.09.286.

D'Acunto B., Esposito G., Frunzo L., Mattei M.R., Pirozzi F., 2016. Mathematical modeling of heavy metal biosorption in multispecies biofilms. *J. Environ. Eng.*, 142, C4015020. DOI: 10.1061/(ASCE)EE.1943-7870.0001052.

Głowacka B., Chrzęszczyk D., Konopka T.P., 2019. The prevalence and severity of periodontitis in a Polish cross-sectional gerodontological study. *J. Stoma.*, 72, 193–201. DOI: 10.5114/jos.2019.93324.

Klapper I., Dockery J., 2010. Mathematical description of microbial biofilms. *SIAM Rev.*, 52, 221–265. DOI: 10.1137/080739720.

Lasserre J.F., Brecx M.C., Toma S., 2018. Oral microbes, biofilms and their role in periodontal and peri-implant diseases. *Materials*, 11, 1802. DOI: 10.3390/ma11101802.

Moscicka-Studzinska A., Ciach T., 2012. Mathematical modelling of buccal iontophoretic drug delivery system. *Chem. Eng. Sci.*, 80, 182–187. DOI: 10.1016/j.ces.2012.05.048.

Patini R., Staderini E., Lajolo C., Lopetuso L., Mohammed H., Rimondini L., Rocchetti V., Franceschi F., Cordaro M., Gallenzi P., 2018. Relationship between oral microbiota and periodontal disease: a systematic review. *Eur. Rev. Med. Pharmacol. Sci.*, 22, 5775–5788. DOI: 10.26355/eurrev_201809_15903.

Picioreanu C., Van Loosdrecht M.C., Heijnen J.J., 2000. Effect of diffusive and convective substrate transport on biofilm structure formation: a two-dimensional modeling study. *Biotechnol. Bioeng.*, 69, 504–515. DOI: 10.1002/1097-0290(20000905)69:5%3C504::AID-BIT5%3E3.0.CO;2-S.

Pjanović R., Bošković-Vragolović N., Veljković-Giga J., Garić-Grulović R., Pejanović S., Bugarski B., 2010. Diffusion of drugs from hydrogels and liposomes as drug carriers. *J. Chem. Technol. Biotechnol.*, 85, 693–698. DOI: 10.1002/jctb.2357.

Reinscheid U.M., 2006. Direct determination of ciprofloxacin in admixtures with metronidazol and ampicillin by NMR. *J. Pharm. Biomed. Anal.*, 40, 447–449. DOI: 10.1016/j.jpba.2005.07.015.

Siepmann J., Siepmann F., 2012. Modeling of diffusion controlled drug delivery. *J. Controlled Release*, 161, 351–362. DOI: 10.1016/j.jconrel.2011.10.006.

Stewart P.S., 1996. Theoretical aspects of antibiotic diffusion into microbial biofilms. *Antimicrob. Agents Chemother.*, 40, 2517–2522. DOI: 10.1128/AAC.40.11.2517.

Trusek A., Grabowski M., Ajayi O., Kijak E., 2023. Hyaluronic acid–alginate homogeneous structures with polylactide coating applied in controlled antibiotic release. *Gels*, 9, 526. DOI: 10.3390/gels9070526.

Vrany J.D., Stewart P.S., Suci P.A., 1997. Comparison of recalcitrance to ciprofloxacin and levofloxacin exhibited by Pseudomonas aeruginosa bofilms displaying rapid-transport characteristics. *Antimicrob. Agents Chemother.*, 41, 1352–1358. DOI: 10.1128/AAC.41.6.1352.

Wang Q., Zhang T., 2010. Review of mathematical models for biofilms. *Solid State Commun.*, 150, 1009–1022. DOI: 10.1016/j.ssc.2010.01.021.

Wang W., Wang W., Zhang X., Wang D., 2002. Adsorption of p-chlorophenol by biofilm components. *Water Research*, 36, 551–560. DOI: 10.1016/S0043-1354(01)00267-6.

World Health Organization, 2025. Oral health. Available at: https://www.who.int/news-room/fact-sheets/detail/oral-health.